JOURNAL OF GEOPHYSICAL RESEARCH, VOL. 117, A04212, doi:10.1029/2011JA017359, 2012

Thin current sheets in the presence of a guiding magnetic field in Earth's magnetosphere

H. V. Malova,[1,2] V. Y. Popov,[3,4] O. V. Mingalev,[5] I. V. Mingalev,[5] M. N. Mel'nik,[5] A. V. Artemyev,[6] A. A. Petrukovich,[6] D. C. Delcourt,[7] C. Shen,[8] and L. M. Zelenyi[6]

Received 11 November 2011; revised 24 January 2012; accepted 24 February 2012; published 12 April 2012.

[1] A self-consistent theory of relatively thin anisotropic current sheets (TCS) in collisionless plasma is developed, taking into account the presence of a guiding field B_y (all notations are used in the GSM coordinate system). TCS configurations with a finite value of guiding field B_y are often observed in Earth's magnetotail and are typical for Earth's magnetopause. A characteristic signature of such configurations is the existence of a magnetic field component along the direction of TCS current. A general case is considered in this paper with global sheared magnetic field B_y = *const.* Analytical and numerical (particle-in-cell) models for such plasma equilibria are analyzed and compared with each other as well as with Cluster observations. It is shown that, in contrast to the case with $B_y = 0$, the character of "particle-current sheet" interaction is drastically changed in the case of a global magnetic shear. Specifically, serpentine-like parts of ion trajectories in the neutral plane become more tortuous, leading to a thicker current sheet. The reflection coefficient of particles coming from northern and southern sources also becomes asymmetric and depends upon the value of the B_y component. As a result, the degree of asymmetry of magnetic field, plasma, and current density profiles appears characteristic of current sheets with a constant B_y. In addition, in the presence of nonzero guiding field, the curvature current of electrons in the center of the current sheet decreases, yielding an effective thickening of the sheet. Implications of these results for current sheets in Earth's magnetosphere are discussed.

Citation: Malova, H. V., V. Y. Popov, O. V. Mingalev, I. V. Mingalev, M. N. Mel'nik, A. V. Artemyev, A. A. Petrukovich, D. C. Delcourt, C. Shen, and L. M. Zelenyi (2012), Thin current sheets in the presence of a guiding magnetic field in Earth's magnetosphere, *J. Geophys. Res.*, *117*, A04212, doi:10.1029/2011JA017359.

1. Introduction

[2] Thin current sheets (TCS) with thicknesses of about one or a few ion gyroradii ρ_i play a key role in the collisionless plasma of Earth's magnetosphere. Numerous in situ measurements by CLUSTER, GEOTAIL or THEMIS [e.g., *Sergeev et al.*, 2003; *Asano et al.*, 2004; *Runov et al.*, 2009; *Baumjohann et al.*, 2007], laboratory experiments [e.g., *Yamada et al.*, 2010; *Frank et al.*, 2008] and observations of various astrophysical objects [e.g., *Arons*, 2011] confirm that these magnetic and plasma structures are responsible for accumulation and release of stored magnetic energy in a variety of cosmic configurations. Different types of magnetic topology deformations characteristic of a guiding magnetic B_y component can be observed in magnetotail current sheet [e.g., *Petrukovich*, 2011; *Shen et al.*, 2008a, 2008b] such as twisting, tilting, bending and others. Despite a long history of investigation of current layers in space plasma, this subject becomes especially important nowadays because of the necessity to understand the large variety of in situ TCS observations by various space crafts.

[3] Kinetic models are more appropriate for TCS description in comparison with MHD because the characteristic scale of the observed structures often is comparable with ion Larmor radii and particles can be nonmagnetized inside the TCS. The first (and most famous) model of self-consistent current sheet was proposed by *Harris* [1962]. It is a mathematically simple kinetic model of current configuration where magnetic fields with two opposite directions are supported by the diamagnetic current in an almost isotropic plasma concentrated near the neutral plane. The normal magnetic field component B_z was not explicitly taken into

[1]Skobeltsyn Institute of Nuclear Physics, Lomonosov Moscow State University, Moscow, Russia.
[2]Also at Space Research Institute, RAS, Moscow, Russia.
[3]Physics Department, Lomonosov Moscow State University, Moscow, Russia.
[4]Also at Space Research Institute, RAS, Moscow, Russia.
[5]Polar Geophysical Institute, Cola Scientific Center, Murmansk, Russia.
[6]Space Research Institute of Russian Academy of Sciences, Moscow, Russia.
[7]Laboratoire de Physique des Plasmas, Ecole Polytechnique, CNRS, Observatoire de Saint-Maur, Saint Maur des Fosses, France.
[8]Center for Space Science and Applied Research, National Space Science Center, Chinese Academy of Sciences, Beijing, China.

0148-0227/12/2011JA017359

account in this model. Nevertheless, it was subsequently considered for the description of current sheets at the magnetopause and in the magnetotail during quiet conditions when the plasma is almost isotropic. The one-dimensional Harris model has been further generalized to the two-dimensional case with self-consistent tangential and normal components of the magnetic field [e.g., *Schindler*, 1972; *Kan*, 1973] that describe relatively thick current layers with thicknesses much larger than the ion Larmor radii.

[4] When the Harris model was used to investigate TCS stability, a number of questions emerged. As an example, the Harris current sheet was found to be unstable for tearing perturbation [e.g., *Coppi et al.*, 1966; *Schindler*, 1974]. But if one takes into account the small normal component of the magnetic field B_z that exists in the magnetotail owing to Earth's dipole field, such current sheet becomes absolutely stable in a linear approximation owing to the effect of electron compressibility (electrons are magnetized by a very small B_z component) [e.g., *Pellat et al.*, 1991]. This paradoxical situation (namely, theory is unable to explain the formation of X line in the magnetotail as manifested in many observations) existed for almost two decades [e.g., *Galeev and Zelenyi*, 1976; *Kuznetsova and Zelenyi*, 1991, *Sitnov et al.*, 1997; *Brittnacher et al.*, 1998]. The necessity to develop new TCS models with normal magnetic component B_z became clearly apparent.

[5] The application of the theory of quasi-adiabatic invariants of motion [e.g., *Büchner and Zelenyi*, 1989] led to the development of a separate class of 1-D models with a self-consistent tangential magnetic field component and a constant normal magnetic field [*Kropotkin and Domrin*, 1996; *Kropotkin et al.*, 1997; *Sitnov et al.*, 2000; *Zelenyi et al.*, 2000]. Unlike models with isotropic pressure where the tension of magnetic lines is counterbalanced by a gradient of plasma pressure along the current sheet, the balance between magnetic tension and plasma pressure in these models is provided by the anisotropy and/or nongyrotropy of the pressure tensor, that is, by the inertia of ions moving across the current sheet. Such models proved to be successful for the description of various TCS types observed in the magnetotail [e.g., *Artemyev et al.*, 2008].

[6] In conjunction with the development of TCS models with nonzero normal component of the magnetic field, another class of models has been developed; that is, models with $B_z = 0$ but with a magnetic shear $B_y \neq 0$ [e.g., *Alpers*, 1971; *Lemaire and Burlaga*, 1976]. These models have often been applied to the description of the magnetopause TCS [see, e.g., *Lee and Kan*, 1979; *Panov et al.*, 2011] and TCS in the solar wind [e.g., *Keyser et al.*, 1996]. A comprehensive review of these plasma equilibria has been made by *Roth et al.* [1996]. Because TCSs are important elements of planetary magnetospheres that play the role of reservoirs of magnetic energy which can be accumulated and subsequently released in the form of kinetic energy of accelerated plasma streams [see, e.g., *Baker et al.*, 1996; *Zelenyi et al.*, 2008; *Angelopoulos et al.*, 2008], we consider the investigation of TCS with magnetic shear to be an important and up-to-date task. To our knowledge, no analysis of self-consistent sheet structures with $B_y \neq 0$ has been presented thus far. Earlier investigations of the shear influence on particle dynamics in current sheets were made with the help of particle tracing for relatively thick current sheet [e.g., *Birn and Hesse*, 1994; *Larson and Kaufmann*, 1996; *Hilmer and Voigt*, 1987] as well as in TCSs [*Kaufmann et al.*, 1997; *Holland et al.*, 1996; *Delcourt and Belmont*, 1998; *Delcourt et al.*, 2000]. In the study of *Delcourt et al.* [2000], the particle dynamics was analyzed over a wide range of parameters, from the magnetized regime to the unmagnetized one. It was shown that particle scattering in the presence of a guiding field is asymmetric and depends upon the position of a plasma source with respect to the current sheet plane. *Kaufmann et al.* [1994] also put forward that the presence of guiding field leads to the destruction of energy resonances in particle scattering.

[7] However, there are many studies of magnetic reconnection in sheared configurations where the quadrupole system of magnetic Hall components has been observed [e.g., *Nakamura et al.*, 2008; *Runov et al.*, 2003; *Shay et al.*, 2007]. The role of electron currents in the formation of Hall reconnection structures is well known but for TCS plasma equilibria, this question was not properly addressed. Self-consistent one-dimensional hybrid simulations of a field reversal in the near-Earth magnetotail have shown that an odd magnetic component B_y appears in the center of CS accompanied by a "bell-shaped" longitudinal current density [e.g., *Richardson and Chapman*, 1994; *Chapman and Mouikis*, 1996].

[8] An important result that motivates the present study was provided by *Rong et al.* [2011] in a study devoted to statistical analysis of the shear magnetic component in Earth's magnetotail. In this latter study, it is shown that two characteristic cases can be distinguished in spacecraft observations: (1) global (almost constant) current aligned magnetic field component in the magnetotail, and (2) local magnetic shear component that changes its sign across the current layer and tends toward minimum values at its edges. In the present study, we investigate in detail the first case, that is, the structure of self-consistent configurations for the externally driven sheared magnetic field. The second case of magnetic shear (with unipolar and bipolar B_y modes across CS) supported by longitudinal currents in TCS will be considered in a future study.

[9] The formation of asymmetric TCS profiles [e.g., *Runov et al.*, 2006] is an interesting problem of its own that is not well understood at present. One possible mechanism responsible for this asymmetry was proposed based standard kinetic TCS model taking into account the natural asymmetry of plasma sources in different hemispheres [*Malova et al.*, 2007; *Mingalev et al.*, 2009]. Here, we suggest another possible mechanism for the formation of skewed plasma configurations in the magnetotail. This latter mechanism relies on asymmetric particle scattering at TCS in the presence of a global sheared magnetic component. In this study, we generalize two complementary models of anisotropic TCSs: (1) an analytical model based on a solution of Vlasov-Maxwell equations [e.g., *Zelenyi et al.*, 2004], and (2) a particle-in-cell (PIC) numerical model [*Mingalev et al.*, 2007, 2009].

2. Particle Dynamics in the Sheared Magnetotail Current Sheet

[10] As a preliminary comment, it is useful to compare the present results for a sheared configuration with the case

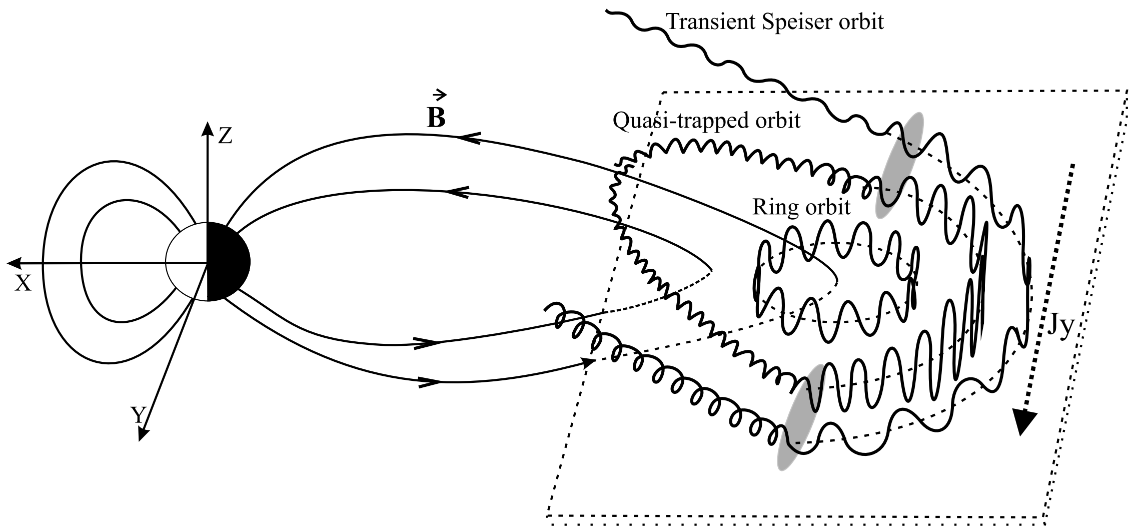

Figure 1. Schematic view of Earth's magnetotail with stretched magnetic field lines in the nightside sector and characteristic dynamical regimes: Speiser particles and quasi-trapped and trapped particles at ring orbits. The direction of the cross-tail current j_y (dashed line) is shown in GSM system of reference. Regions marked in gray indicate the separatrix of particle motion where particles change their motion between regimes of crossing and noncrossing of the TCS midplane.

$B_y = 0$ where particle dynamics is well known [e.g., *Büchner and Zelenyi*, 1989; *Chen*, 1992]. Since the TCS thickness L is much larger than the electron gyroradius ($L \sim \rho_i \gg \rho_e$), one can consider the electrons as totally magnetized. As for ions, there are three basic types of trajectories: (1) Speiser ions [e.g., *Speiser*, 1965] with open orbits that are going from/to infinity, (2) quasi-trapped ions that can be temporarily trapped within TCS and experience many oscillations before being detrapped, (3) ions with closed (totally integrable) orbits that do not scatter and do not leave the TCS region. These three types of ion orbits are schematically shown in Figure 1. According to analytical models [e.g., *Zelenyi et al.*, 2000] and spacecraft observations [e.g., *Artemyev et al.*, 2011], Speiser ions in Figure 1 are the main current carriers in the TCS. As for quasi-trapped and trapped ions, they do not carry any net current because their orbits are closed but the local current they carry can significantly alter the CS structure. Indeed, owing to strongly curved serpentine-like motions near the neutral plane, these latter ions can support local currents that are directed oppositely to the general cross-tail current carried by Speiser particles [e.g., *Zelenyi et al.*, 2000, 2002a, 2002b, 2003].

[11] In the following, we use the standard GSM coordinate system where the X axis is directed from the center of Earth toward the Sun, the Y axis is along the "dawn-dusk" direction, and the Z axis is in the south-north one. In the deHoffmann-Teller reference frame where the dawn-dusk electric field cancels, the remaining electric field only has one component in the Z direction, that is, $\mathbf{E} = \{0, 0, E_z\}$. The particle equation of motion then has the form:

$$m\frac{d^2\mathbf{r}}{dt} = \frac{e}{c}[\mathbf{v} \times \mathbf{B}] + e\mathbf{E} \qquad (1)$$

The above component E_z is the ambipolar electric field that appears owing to the different dynamics of ions and electrons. Also, $\mathbf{B} = \{B_x, B_{y0}, B_{z0}\}$ is the magnetic field with constant components B_{y0}, B_{z0}. Conservation of the total particle energy immediately follows from integration of (1) with potential field $\mathbf{E} = -\nabla\varphi$:

$$\frac{mv^2}{2} + e\varphi = const \equiv W_0 \qquad (2)$$

Here, one has $v^2 = v_x^2 + v_y^2 + v_z^2$ while $W_0 = mv_0^2/2$ is the total particle energy. In this configuration, the generalized momentum P_{y0} is also conserved:

$$P_{y0} \equiv mv_{y0} = mv_y + \frac{e}{c}\left(B_z x - \int_0^z B_x(z'')dz''\right) \qquad (3)$$

Here, equations (2)–(3) are exact integrals of the motion.

[12] It has been shown in previous studies [e.g., *Sonnerup*, 1971; *Büchner and Zelenyi*, 1989] that the third (approximate) integral of motion $I_z = \frac{1}{2\pi}\oint mv_z dz$ is also conserved during ion motion across the CS. That is, when ions are traveling toward the CS midplane, they cross a separatrix (regions coded in gray in Figure 1) that separates two different dynamical regimes, namely, crossing and noncrossing of the tail midplane. In the course of these separatrix traversals, small quasi-random jumps of invariant ΔI_z occur [e.g., *Neishtadt*, 1987] for both Speiser particles and quasi-trapped particles:

$$\Delta I_z \cong \kappa \ln 2 \left|\sin\theta_{sep}\right| \qquad (4)$$

The parameter of adiabaticity $\kappa = \sqrt{R_c/\rho_{\max}}$ in (4) characterizes the particle motion. Here, $\rho_{\max}$ is the maximum ion gyroradius and R_c is the minimum curvature radius of the magnetic lines while θ_{sep} is the phase of the particles at the separatrix. In the simplest model of magnetic field

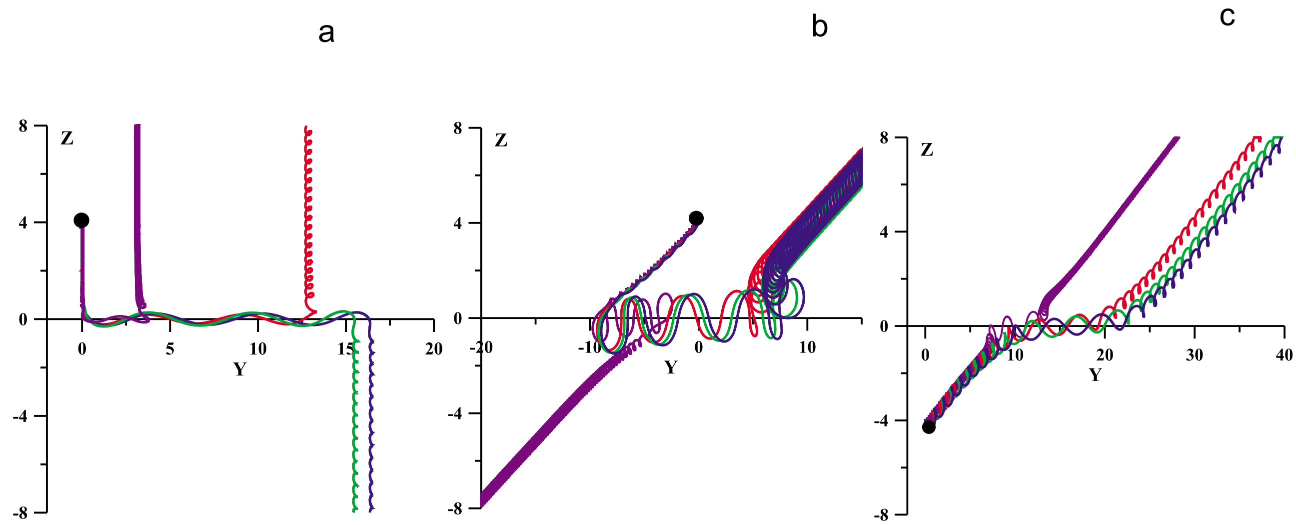

Figure 2. *X-Z* projections of four ion trajectories in TCS: (a) for a magnetic configuration without magnetic shear $B_{y0}/B_{x0} = 0.0$ ($\kappa = 0.12$), (b) in the presence of a guiding field with a relative value $B_{y0}/B_{x0} = 0.2$ for particles from the northern source, and (c) for conditions similar to Figure 2b but for particles launched from the southern source. Here B_{y0} is the value of the guiding magnetic field, and B_{x0} is that of the tangential magnetic field at the TCS edges. Space variables are normalized to the ion Larmor radius. Initial energies are identical, while pitch angles are θ_0 = 0.15 (dark blue line), 0.35 (green line), 0.65 (red line) and 1.35 (violet line).

reversal $\mathbf{B} = \{B_{x0}(z/L), 0, B_{z0}\}$ the value of this adiabaticity parameter is $\kappa = (B_{z0}/B_{x0})\sqrt{L/\rho_i}$ where L is the CS thickness, ρ_i, the ion Larmor radius and $B_0 = \sqrt{B_{x0}^2 + B_{z0}^2}$. When $\kappa \gg 1$, the motion of charged particles can be described by the guiding center theory. At κ of the order of 1, the particle motion becomes stochastic and experience large jumps $\Delta I_z \sim I_z$. This latter dynamical chaos in the magnetotail has been described for instance by *Büchner and Zelenyi* [1986, 1989] and *Chen and Palmadesso* [1986]. Finally, when $\kappa \ll 1$, jumps of the adiabatic invariant of motion ΔI_z become smaller than the value of the invariant I_z itself, and the particle motion can be considered as quasi-adiabatic [e.g., *Büchner and Zelenyi*, 1989]. This quasi-adiabatic regime of motion therefore consists of two regular segments before and after separatrix crossings during which $I_z \approx const$ and which are separated by small stochastic jumps ΔI_z at separatrix crossings. One important property of quasi-adiabatic motion is the existence of resonances during particle interaction with the current sheet depending upon energy or, in dimensionless form, depending on parameter κ [e.g., *Chen and Palmadesso*, 1986; *Burkhart and Chen*, 1991; *Büchner and Zelenyi*, 1991; *Ashour-Abdalla et al.*, 1993]. At resonances $\kappa = \kappa_{res}$, the jumps of invariant I_z at entry of particles into CS are exactly compensated by the one at exit and, as a result, particles leave CS without any scattering. This property explains the appearance of accelerated plasma flows along magnetic field lines, or so-called "beamlets" [e.g., *Ashour-Abdalla et al.*, 1992; *Keiling et al.*, 2004; *Zelenyi et al.*, 2007]. For other nonresonant conditions, the particle motion can be considered as diffusion in the I_z space.

[13] It should be noted here that the above expression for the jumps of adiabatic invariants (4) was obtained for the case $B_y = 0$. From a general viewpoint, one expects these jumps to depend upon the value B_{y0} at the edges of CS. In the presence of sheared magnetic field, the effective value of the parameter κ is increased. More specifically, it was estimated as $\kappa_y = \kappa[1 + (B_{y0}/B_{z0})^2]^{3/4}$ [*Büchner and Zelenyi*, 1991] in the case of a parabolic field reversal. In the present study, we will neglect this dependence on B_y which is justified for the small values of guiding field ($B_{y0} \ll B_0$) considered. Accordingly, we assume that estimate (4) can be applied for our quasi-adiabatic model even for $B_y \neq 0$.

[14] As mentioned above, particle dynamics in current sheets with magnetic shear remains largely unexplored. *Kaufmann et al.* [1994] established that, in the presence of guiding field, pitch angle scattering is enhanced. In terms of quasi-adiabatic theory, this may be viewed as the result of resonance destruction by the B_y field. This result is at variance with those of *Chapman and Rowlands* [1998] who showed that adiabatic integrals of particle motion are generally conserved in the presence of magnetic shear. Still, at specific energies, the invariant surfaces of trapped motion in phase space can be destroyed, and these regions can then be occupied by transient particles. In other words, constant B_y possibly leads to particle detrapping from the system.

[15] We first examine qualitatively the influence of magnetic shear on a few specific particle orbits. Examples of trajectories with different pitch angles are shown in Figure 2 that illustrates the evolution of transient ion dynamics. Here, particles are launched from Northern and Southern Hemispheres without (Figure 2a) and with (Figures 2b–2c) guiding field $B_{y0}/B_{x0} = 0.2$. Only {X-Z} projections of the orbits are shown, the particle initial position being indicated by closed black circles. A notable feature in Figures 2a, 2b, and 2c is the varying height of particle deviation from the neutral plane during serpentine-like motion. In the presence of a guiding field, this deviation occurs at a large Z height in Figure 2b because trajectories are more twisted than in Figure 2a.

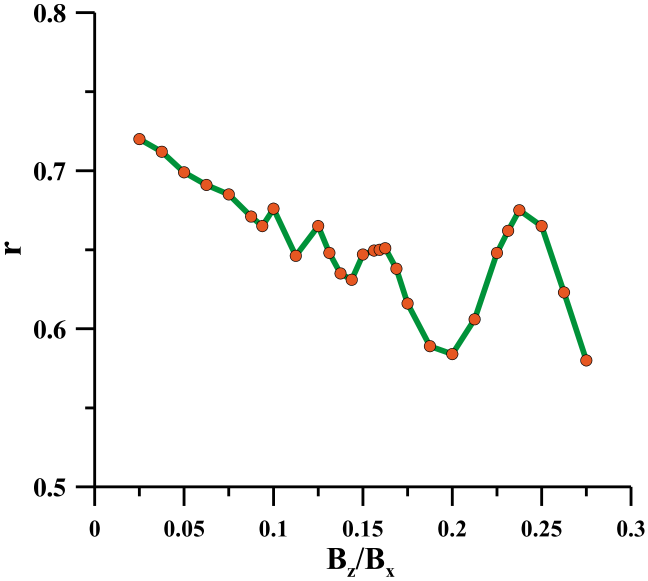

Figure 3. Particle reflection coefficient r from TCS as a function of B_z component of the magnetic field in the presence of zero guiding field. Red circles show the computed r values.

From this qualitative result, one may suspect that the CS thickness which is determined by the length scale of serpentine motion may be larger in sheared configurations. In Figure 2c, particle deviation from the CS plane occurs at some intermediate height as compared to Figures 2a and 2b. Figure 2 also reveals that particle scattering does not change significantly in the presence of nonzero positive B_y component if particles are launched from the Northern Hemisphere. In contrast, if particles are launched from the Southern Hemisphere, prominent scattering may occur and particles are preferentially reaching the opposite hemisphere, as apparent from Figure 2c.

[16] Another characteristic of quasi-adiabatic ion dynamics in the sheared CS configuration is the enhanced particle trapping near the CS midplane for ions from the northern source in comparison with those from the southern one. The trajectories of quasi-trapped particles also become more and more tangled depending upon the value of the guiding field. Note that, in the case of $B_y < 0$, symmetrical results are obtained with respect to the X-Y plane. The comparison of Figures 2a–2c demonstrates that the general topology of ion trajectories is conserved in all cases. More specifically, the topology of Speiser orbits is conserved up to values $B_{y0}/B_{x0} \sim 0.4 \sim 0.5$ according to our numerical experiment. For larger values of B_y, Speiser orbits are transformed into quasi-trapped ones that cannot support a net cross-tail current. For $B_{y0}/B_{x0} \sim 1$, almost all particles in the system are magnetized by the field B_y and the current sheet is now supported by the drift motions of the particles near the current sheet center.

[17] To study the bulk properties of particle scattering, we launched an ensemble of particles having a shifted Maxwellian distribution function with an average speed parallel to the magnetic field lines at the edges of CS. In these simulations, $2 \cdot 10^5$ ions were traced for different values of B_z (B_{z0} = 0.5, 1, 2, 3, 4 nT) and for a magnetic field at the edges of TCS $B_{x0} \simeq 20\ nT$. Here, we considered $B_y(z) \equiv 0$. The Maxwellian ion distribution is such that $V_T/V_D = 0.5$ (V_T and V_D being the thermal and flow plasma velocities, respectively) and the temperature is $T = 4\ keV$. We determined the reflection coefficient as the number of particles that return back to the source hemisphere (over the entire time of tracing) normalized to the total number of particles that are launched. The dependence of this reflection coefficient upon the B_z value for $B_y(z) \equiv 0$ and $B_{x0} = 20\ nT$ is shown in Figure 3. Not surprisingly, Figure 3 demonstrates that reflection coefficients for particles started in the Northern and Southern Hemispheres are equal, their values being in the 0.6–0.75 interval. It can be seen in Figure 3 that the reflection coefficient for a typical magnetotail ratio $B_{z0}/B_{x0} \approx 0.05$ is about 0.7. Note also the resonant character of the reflection coefficient profile. That is, four minima can be seen in Figure 3 that coincide with the ion resonance reported by *Chen* [1992]. In this latter study, a phenomenological dependence of adiabatic parameter κ on resonance number N was obtained as $\kappa = 2^{-1/4}/(N + 0.6)$. Resonance occurs when the ratio ω_z/ω_x acquires some integer value N = 1,2,3,… (ω_z and ω_x being the particle oscillation frequencies in Z and X directions, respectively).

[18] Figure 4 shows the variation of the reflection coefficients for different magnetic shears B_y and for a fixed value of B_z. It can be seen in Figure 4 that the reflection coefficient for particles originating from the northern source does not depend upon the B_y value. In contrast, the coefficient r for particles originating from the southern source decreases in inverse proportion to B_y, reaching about 0.3 for B_{y0}/B_{x0} = 0.3. This feature confirms the qualitative result of Figure 2 where most transient particles from the southern source were found to cross the current sheet without any scattering and gain access to the opposite hemisphere. It can therefore be anticipated that an increase

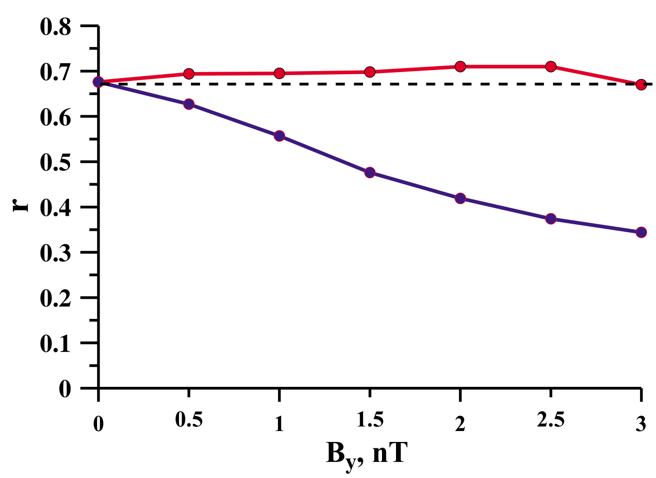

Figure 4. Particle reflection coefficient from TCS for plasma sources located in Northern and Southern Hemispheres as function of B_{y0} (see section 6 for PIC simulation results). The following parameters were used in the simulations: $B_{z0} = 1\ nT$, $B_{x0} = 20\ nT$.

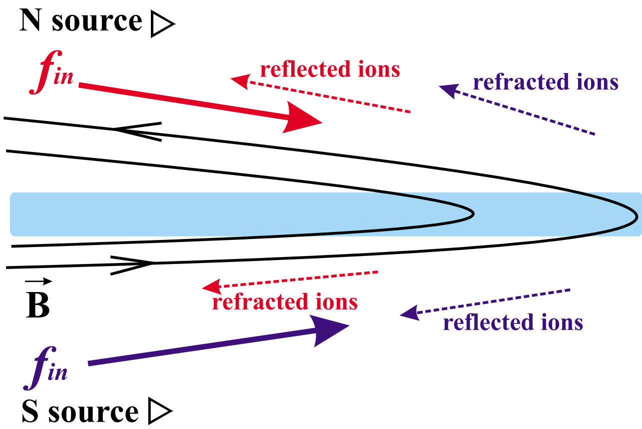

Figure 5. Sketch of the modeling scheme; namely, particles streaming from northern and southern sources (N and S, respectively) toward TCS (light blue region) are either reflected from TCS or refracted through TCS (the direction of streams is shown by dashed lines of corresponding color). The asymmetric shape of TCS is a result of asymmetric particle scattering.

of the guiding field should lead to an asymmetry of the TCS structure because of the asymmetry of the plasma density. For the case $\kappa \geq 1$, the scattering asymmetry has been explained by *Delcourt et al.* [2000] in terms of perturbation of the gyromotion by an impulsive centrifugal force acting in the vicinity of the CS plane. Here, a nonzero B_y leads to a rotation of the centrifugal impulse in the gyration plane. The effect is either attenuated or enhanced when the direction of this rotation opposes or goes in the same direction as the gyromotion, respectively. As a result, particles originating from opposite hemispheres behave quite distinctly, experiencing for instance large or negligible magnetic moment changes depending on the direction of particle propagation. The results above suggest that the presence of a guiding field should lead to some asymmetry of thin current sheets ($\kappa \ll 1$). In the following, we explore this result further using both analytical and numerical self-consistent models.

3. General Description of the Analytical Model

[19] In this section, we present a generalization of the analytical self-consistent model of thin current sheet in collisionless plasma [*Zelenyi et al.*, 2004] that includes an additional B_y component of the magnetic field. The current sheet is supposed to be quite thin with characteristics depending only upon z coordinate [see, e.g., *Sitnov et al.*, 2000; *Zelenyi et al.*, 2000]. For our 1-D TCS model, we consider all three components of the magnetic field $\mathbf{B} = \{B_x(z), B_y, B_z\}$with $B_y = const_1$ and $B_z = const_2$. As for $B_x(z)$, it changes sign in the equatorial plane $z = 0$. The plasma equilibrium in the current sheet is supported by the balance between tension of the magnetic field lines and finite inertia of the ions [*Zelenyi et al.*, 2000]. When constructing this model, the following general assumptions are made:

[20] 1. Counter-streaming plasma flows from both northern and southern sources similar to the magnetospheric plasma mantle intercept the TCS as illustrated shown in Figure 5. These plasma flows may be reflected or transmitted after interaction with TCS (in the following, these particles are referred to as reflected or refracted, respectively).

[21] 2. The value of the B_y component is significantly smaller than that of B_x. Accordingly, the resulting magnetic field at the TCS center is still too small to magnetize all the incoming ions. As a matter of fact, part of the ion population is demagnetized inside TCS and follows quasi-adiabatic trajectories as discussed above. These particles are responsible for the buildup of the cross-tail current.

[22] 3. The incoming ion population consists of two main groups, namely, Speiser ions and quasi-trapped ions (trapped ions are not considered here). As discussed above, for quasi-adiabatic trajectories, the action integral $I_z = \frac{1}{2\pi}\oint m v_z dz$ is conserved [e.g., *Sonnerup*, 1971; *Whipple et al.*, 1986; *Büchner and Zelenyi*, 1989].

[23] 4. The TCS considered is "thick" for electrons. Therefore, their motion can described with the help of the guiding center approximation. Assuming that the electron motion is fast, we consider their distribution along the magnetic field lines as a Boltzmann one [*Zelenyi et al.*, 2004]. The electron drift current reaches a maximum value in the neutral plane because curvature drifts are maximum inside the TCS where the curvature radius of the magnetic field lines is minimum.

[24] 5. The quasi-neutrality condition $n_i \approx n_e$ is assumed to hold in the model, which allows us to calculate the ambipolar electrostatic field. The large-scale dawn-dusk electric field E_y is removed from our system of equations by transformation into deHoffmann-Teller reference frame that moves earthward with the velocity $v_{dHT} = cE_y/B_z$. The ambipolar electrostatic field $E_z(z)$ that results from the different dynamics of ions and electrons inside TCS is taken into account, whereas one has $E_x = 0$ for this 1-D current sheet model. The detailed description of model equations taking into account electrostatic effects is done in the work of *Zelenyi et al.* [2004].

4. Basic Equations of the Analytical Model

[25] Let us denote the distribution function of northern and southern sources as f_1 and f_2. The particle reflection coefficients will correspondingly be r_1 and r_2. Then, the distribution function of Speiser ions in each hemisphere may be written as:

$$f_{z>0} = \begin{cases} f_1, & v_{II} < 0 \\ r_1 f_1 + (1 - r_2) f_2, & v_{II} > 0 \end{cases} \tag{5}$$

$$f_{z<0} = \begin{cases} r_2 f_2 + (1 - r_1) f_1, & v_{II} < 0 \\ f_2, & v_{II} > 0 \end{cases} \tag{6}$$

The distribution functions of incoming ions have the standard shifted form:

$$f_{1,2}(\vec{v}) = \frac{n_{01,2}}{\left(\sqrt{\pi} V_{T1,2}\right)^3 \left(1 + erf\left(\varepsilon_{1,2}\right)\right)} \exp\left\{-\frac{\left(v_\parallel \pm V_{D1,2}\right)^2 + v_\perp^2}{V_{T1,2}^2}\right\} \tag{7}$$

Here, we use the following notations: $\varepsilon_{1,2} = V_{T1,2}/V_{D1,2}$, $V_{T1,2}$ and $V_{D1,2}$ are thermal and plasma flow velocities, $n_{01,2}$ are plasma densities in the Northern and Southern Hemispheres, and the signs "+" and "−" correspond to flows parallel ($v_{II} > 0$) and antiparallel ($v_{II} < 0$) to the magnetic field direction. Below, we assume that plasma sources have similar parameters; that is, $n_{01} = n_{02} \equiv n_0$, $V_{D1} = V_{D2} \equiv V_D$, $V_{T1} = V_{T2} \equiv V_T$, $\varepsilon_{1,2} \equiv \varepsilon$. However, the values of coefficients r_1 and r_2 are different as shown in Figure 4. The values of refraction coefficients are correspondingly $1 - r_1$ and $1 - r_2$. These coefficients are free parameters of the model, their values being derived from the PIC simulations described below.

[26] TCS equilibria are described in details in the review by *Zelenyi et al.* [2011]. In the following, we focus on the generalization of the system of stationary Vlasov-Maxwell equations in a configuration with magnetic shear:

$$
\begin{aligned}
&df_{1,2}(\mathbf{v}, z)/dt = 0\\
&\frac{dB_x}{dz} = \frac{4\pi}{c}\left\{\int\limits_{V^3} v_y\left[f_{z>0}(\mathbf{v},z) + f_{z<0}(\mathbf{v}, z) + f_{trap}(\mathbf{v},z)\right]d^3v + j_e(z)\right\}\\
&B_x(z)|_{z=L} = B_{x0},\ \varphi(z)|_{z=L} = 0
\end{aligned}
\tag{8}
$$

where B_{x0} is the value of magnetic field outside TCS, φ is the electrostatic potential, j_e is the electron current density, $f_{z>0}$ and $f_{z<0}$ are determined by (5)–(6). For simplicity, the distribution function of quasi-trapped plasma $f_{trap}(\mathbf{v}, z)$ is chosen to be the same for both hemispheres. Such an assumption is motivated by the fact that quasi-trapped particles are bouncing inside TCS, so that their distribution spreads over the domain containing both Northern and Southern Hemispheres. These latter distributions are added in the form of a thermal Maxwellian $f_{trap} \sim \exp\{-v_0^2/V_T^2\}$ that is sewed with the distribution (7) at the point where $v_\parallel \equiv v_0^2 - v_\perp^2 = 0$, v_0 and $v_\perp$ being the total and perpendicular velocities [*Zelenyi et al.*, 2000]. Also, the magnetic moment $\mu \equiv mv_\perp{}^2/2B_0$ and adiabatic invariant I_z are related by the ratio $2\mu B_0/m \approx (\omega_0/m)I_z$ [*Sitnov et al.*, 2000]. Because the distribution function of quasi-trapped particles belongs to the region of large I_z [*Zelenyi et al.*, 2004], that is, at the tail of the distribution as a function of I_z, the density of quasi-trapped population is small in comparison to that of Speiser ions and we do not investigate their effect further. The third equation in (8) represents boundary conditions for both vector and scalar potentials.

[27] Taking into account the integrals of motion (2)–(3), the quasi-adiabatic invariant outside the TCS $I_z = (1/2\pi)\oint mv_z dz = (m/2\pi)\oint\sqrt{v^2 - (2e/m)\varphi - v_x^2 - v_y^2}dz$ in the presence of $B_y \neq 0$ may be written as:

$$
I_z = \frac{2m}{\pi}\int\limits_{z_0}^{z_1}\sqrt{v^2 + \frac{2e}{m}\left(\varphi(z) - \varphi(z')\right) - \left(v_x - \frac{e}{mc}B_y(z - z')\right)^2 - \left(v_y + \frac{e}{mc}\int\limits_{z'}^{z}B_x(z'')dz''\right)^2}\,dz \tag{9}
$$

The limits of integrations over z of this contour integral are determined as solutions of the equation for turning points $v_z = 0$

$$
-\frac{e}{mc}\int\limits_{z}^{z_{0,1}} B_x(z'')dz'' = v_y \pm\sqrt{v^2 + \frac{2e}{m}\left(\varphi(z) - \varphi(z_{0,1})\right) - \left(v_x + \frac{e}{mc}B_y\left(z - z_{0,1}\right)\right)^2} \tag{10}
$$

Using the relation between particle magnetic moment μ and adiabatic invariant I_z outside the TCS $\mu = (e/2mc)I_z$ [*Kropotkin et al.*, 1997], one can rewrite the source distribution function in terms of invariants of motion $\{v_0, I_z\}$. Using the Liouville theorem $df_{1,2}/dt = 0$, we can calculate this distribution function for any point of the phase space trajectories [*Zelenyi et al.*, 2000]:

$$
f_{1,2}(\mathbf{v}) = \frac{n_0}{(\pi V_T)^3\left(1 + erf\left(\varepsilon^{-1}\right)\right)} \cdot \exp\left\{-\frac{\left(\sqrt{v^2 - \frac{\omega_0}{m}I_z + \frac{2e}{m}\varphi} \pm V_D\right)^2 + \frac{\omega_0}{m}I_z}{V_T^2}\right\} \tag{11}
$$

This distribution function for transient ions is valid for values of adiabatic invariant such that $I_z \leq (m/\omega_0)v_0^2$. The same approach is used for the distribution of quasi-trapped particles $f_{qt} \sim \exp\{-[V_D^2 + (\omega_0/m)I_z]/V_T^2\}$. Finally, the second equation in (8) can be transformed to a nonlocal equilibrium equation similar to the Grad-Shafranov one:

$$
\frac{dB_x}{dz} = \frac{4\pi}{c}\left\{\int\limits_{V^3} v_y\left[f_{z>0}(W_0(\mathbf{v}), I_z(\mathbf{v}, z)) + f_{z<0}(W_0(\mathbf{v}), I_z(\mathbf{v}, z)) + f_{qt}\right] \cdot d^3v + j_{ye}(z)\right\} \tag{12}
$$

As for electrons, they are taken into account using the semihydrodynamic description, described in details in the work of *Zelenyi et al.* [2004], where the electron motion within equilibrium thin current sheet is given by equation $\nabla\hat{\mathbf{p}}_\mathbf{e}/n_e = -e(\mathbf{E} + (1/c)[\mathbf{v}\times\mathbf{B}]) - \mu_e\nabla B$. Here the last term is the repulsive diamagnetic force acting on the electrons with magnetic moment μ_e, $\hat{\mathbf{p}}_e$ is the tensor of electron pressure, electron and ion densities are equal ($n_e = n_i$) owing to quasi-neutrality condition. In a frame of this approach a fluid approach is used to describe the electron motion across the magnetic field lines and a guiding center approximation is applied for the parallel motion. Pressure anisotropy plays an important role in the generation of narrow though intense electron currents in our configuration with a strongly curved

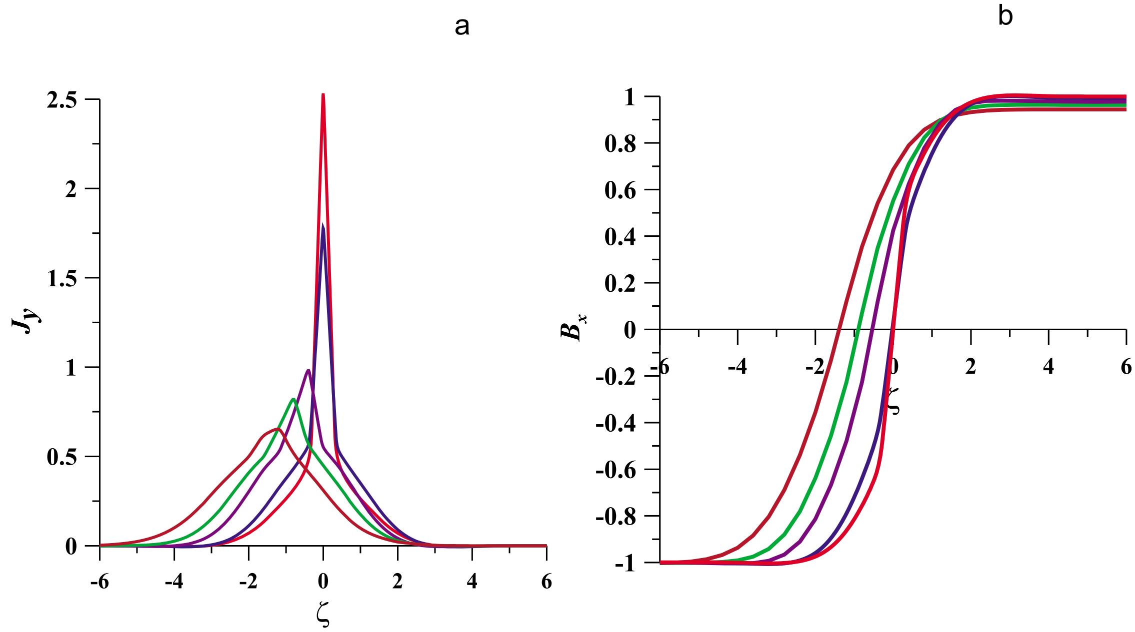

Figure 6. (a) Dimensionless cross-tail current density and (b) magnetic field in TCS for different values of the guiding field B_{y0} and $\varepsilon = 0.1$. The coefficient B_{y0}/B_{x0} is set to 0.0 (red line), 0.1 (blue line), 0.2 (violet line), 0.3 (green line), and 0.4 (brown line).

magnetic field lines. The presence of B_y component results into a magnetic field inclination with respect to the equatorial plane (with inclination angle $\alpha = arctg(B_y/B_z)$). An electric current j_z appears in the system owing to the particle drifts directed orthogonally to the magnetic field lines. We assume that the ambipolar electrostatic field directed along these magnetic field lines supports the parallel currents $j_\parallel$. As a result, the net current in the z direction that consists of two terms $j_z = -j_\perp \sin\alpha + j_\parallel \cos\alpha$ ($j_\perp$ being the drift electron current perpendicular to the magnetic field lines), should vanish for one-dimensional configurations (i.e., $\partial/\partial x = \partial/\partial y = 0$) as is the case here. This is because $j_z = (c/4\pi)(\partial B_y/\partial x - \partial B_x/\partial y) \equiv 0$. Finally, taking into account the condition $j_z = 0$, the expression for the cross-tail current j_{ye} in (8) and (12) can be simplified as:

$$j_{ye} = j_\perp \cos\alpha + j_\parallel \sin\alpha = j_\perp / \cos\alpha \qquad (13)$$

5. Results of the Analytical Model

[28] In the following analytical calculations, r_1 was chosen constant and equal to 0.7 consistently with PIC simulation results (see below). As shown in Figure 4, the coefficient r_2 was decreased linearly from 0.7 at $B_{y0}/B_{x0} = 0.0$ down to $r_2 = 0.3$ at $B_{y0}/B_{x0} = 0.3$ (this ratio value corresponds to $B_{y0}/B_z = 1.5$ for $B_z/B_{x0} = 0.2$ in PIC simulations). We also use dimensionless variables, namely, Z coordinate $\zeta = z\omega_0/\varepsilon^{4/3} V_D$, magnetic field $B_{x,y,z} = \tilde{B}_{x,y,z}/B_{x0}$, plasma density $n = \tilde{n}/N_0$, and current density $J_y = J_{yd}/en_0 v_D \varepsilon^{2/3}$ [*Zelenyi et al.*, 2004], J_{yd} and $\tilde{B}_{x,y,z}$ being the dimensional values of current density and magnetic components.

[29] Figure 6 shows the self-consistent profiles of normalized current density $j_y(z)$, and magnetic field component $B_x(z)$ for different values of B_{y0} component. These profiles were obtained using (8)–(13) and including electrostatic effects. Figure 7 also presents the corresponding profile of plasma density. Several features of interest are noticeable. First, in accordance with Figures 2b and 2c that display the changes of ion trajectories for $B_y \neq 0$, TCS becomes much thicker for larger values of guiding magnetic field. This is due to the distortion of ion trajectories when the meandering

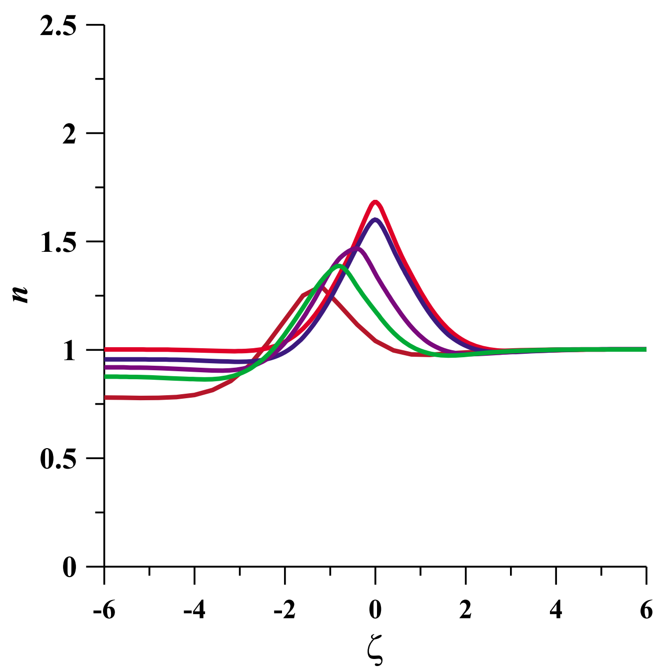

Figure 7. Self-consistent TCS plasma density profiles for different values of guiding field. The format is identical to that of Figure 6.

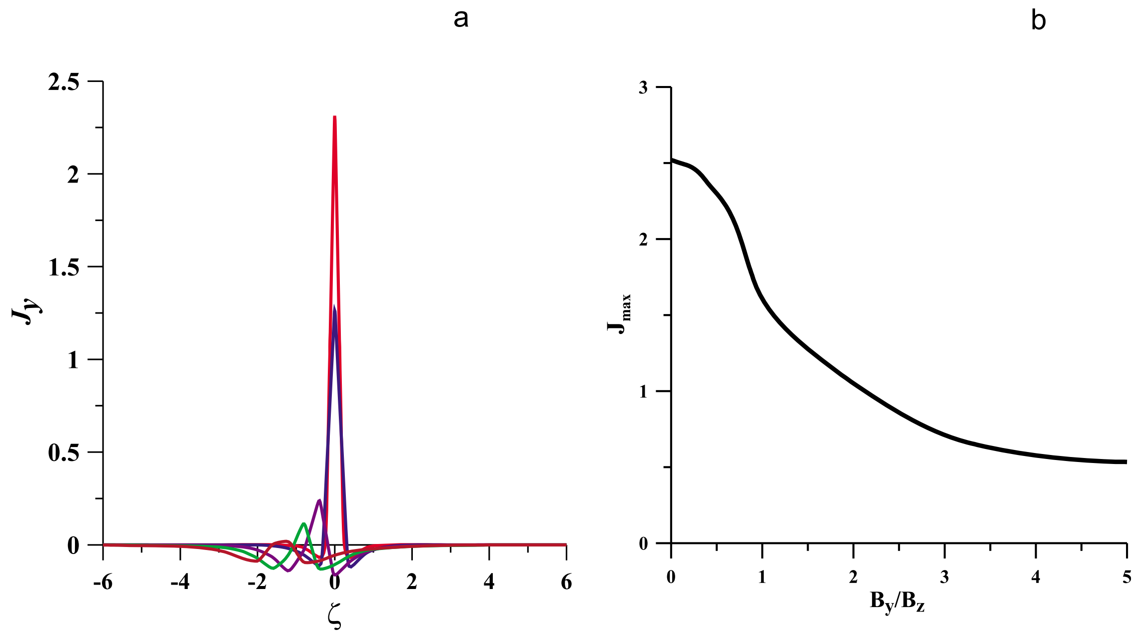

Figure 8. Profiles of electron current and total current density in TCS for different values of the sheared magnetic field: (a) cross-tail profiles of electron current for different B_{y0} (format is identical to that in Figure 6) and (b) maximum value of the total current density as a function of the B_{y0} value.

parts become more tangled. The amplitude of the cross-tail current decreases while TCS thickness increases. Second, an asymmetry of plasma density profiles (Figure 7) in the north-south direction is apparent that depends upon the value of shear magnetic field component. This asymmetry develops as a result of different reflection coefficients that depend upon the value of B_{y0}. The profiles of current density and magnetic field in TCS are, correspondingly, asymmetrical as well. The formation mechanism of this asymmetry here differs from that investigated by *Malova et al.* [2007] where asymmetrical plasma sources were considered. For sheared magnetic field configurations, asymmetry appears even in the case of symmetrical sources and is due to different reflection coefficients. More specifically, the serpentine motion of Speiser ions near the neutral plane supports the stable "bell-shaped" current density at the TCS center. At the edges of TCS, magnetized particles that are not crossing the midplane experience substantial diamagnetic drifts in the negative Y direction, yielding small negative currents or "diamagnetic wings" at the edges of TCS as described by *Zelenyi et al.* [2000]. Since the plasma density is larger in the Northern Hemisphere than in the Southern Hemisphere, the reduction of the cross-tail current owing to the negative diamagnetic currents is larger, and an overall southward shift of the current profile occurs.

[30] Another feature of interest in Figure 7 concerns the electron current that is supported mainly by curvature drift. Taking into account the proportionality of this electron current to the inverse of the magnetic field line curvature radius R_c^{-1} [e.g., *Zelenyi et al.*, 2004] as well as the relation $R_c \sim \kappa^2$ and the estimate of parameter κ_y by *Büchner and Zelenyi* [1991] (see section 2), one can estimate the electron current density as $j_e \sim (1 + (B_{y0}/B_{z0})^2)^{-1}$. Figure 8a indeed displays a fast decrease of the electron current density as B_y increases. For B_{y0}/B_{x0} of about 0.3 and above, the contribution of the electron current to the total one becomes negligible, and the TCS profile is only controlled by the ion motion. Figure 8b shows the dependence of the maximum current density as a function of B_{y0}. It can be seen that for $B_y/B_x \neq 0$ values, this maximum current density decreases when the guiding field increases. For small B_{y0} values, this is due primarily to the decrease of the electron current. For larger B_{y0}, the effect of the ion current decrease also becomes important.

6. Basics of the PIC Model

[31] The analytical results presented above have been compared with those from self-consistent PIC simulations. On this purpose, we developed 1D3V numerical model with one spatial and three velocity coordinates. The general assumptions of this model are identical to those discussed in section 4. The only difference with analytical model is that electrostatic effects were not taken into account in PIC model. Therefore we consider below only ion-dominated sheets. We consider de Hoffman–Teller coordinate system where the external electric field E_y is transformed to zero. Thus in PIC simulation we jointly solve the stationary 1D3V Vlasov equation for protons and 1-D Ampere equation for magnetic field: $v_z \frac{\partial f}{\partial z} + \frac{e}{m_p}\left([\mathbf{v} \times \mathbf{B}], \frac{\partial f}{\partial \mathbf{v}}\right) = 0$, $\frac{dB_x}{dz} = \mu_0 j_y(z)$. The magnetic field and current density in the CS are assumed to have only one self-consistent component; that is, $\mathbf{B}(z) = \left(B_x(z); B_y; B_z\right)$, $\mathbf{j}(z) = \left(0; j_y(z); 0\right)$; B_y and B_z are constant. Below and above CS, the magnetic field is constant: $\mathbf{B}\big|_{z \geq Z_0} = \left(B_x(Z_0); B_y; B_z\right)$, $\mathbf{B}\big|_{z \leq -Z_0} = \left(B_x(-Z_0); B_y; B_z\right)$. Here Z_0 is half of the model region size in Z direction, which is much larger than current sheet half-thickness L. The boundary values of the self-consistent component B_x are defined in terms of their changes across CS $\Delta B_x = B_x(Z_0) - B_x(-Z_0)$;

the change of the $\Pi_{z,z}$ component of the stress tensor $\Delta\Pi_{z,z} = \Pi_{z,z}(Z_0) - \Pi_{z,z}(-Z_0)$ via the relationships $B_x(\pm Z_0) = \mu_0(\Delta\Pi_{z,z}/\Delta B_x) \pm (1/2)\Delta B_x$ follows from condition of the force balance along the Z axis: $\Pi_{z,z}(z) + |B_x(z)|^2/2\mu_0 \equiv$ const.

[32] Current density and the stress tensor components are defined by the formulae

$$\mathbf{j}(z) = e\int \mathbf{v}f(z,\mathbf{v})\,d^3\mathbf{v}, \Pi_{i,k}(z) = m_p\int v_i v_k f(z,\mathbf{v})\,d^3\mathbf{v}.$$

The CS is supported by impinging plasma flows along magnetic field lines from the boundary of the calculation region toward its center. The input parameters of the model are the constant magnetic field components B_z and B_y, plasma flow velocity along magnetic field lines V_D and ion thermal speed V_T of impinging ion flows from magnetosphere plasma mantle, and also the jump ΔB_x of magnetic field component B_x across the sheet. The distribution functions of ions in the impinging ion flows have the form of the Maxwellian distributions:

$$f_{(\pm)}(z,\mathbf{v}) = f_0\left(z,\mathbf{v},n_{(\pm)},T,V_D\right) = \frac{n_{(\pm)}}{\left(V_T\sqrt{2\pi}\right)^3}\exp\left(-\frac{|\,\mathbf{v}-\mathbf{U}(z)|^2}{V_T{}^2}\right) \tag{14}$$

Indexes (+) and (−) signify ion flows, correspondingly, from the northern and southern sources, $n_{(\pm)}$ are corresponding plasma concentrations, T is the ion temperature and V_T is the thermal speed of ions, while $\mathbf{U}(z) = -zV_D\mathbf{b}(z)/|z|$ is the average flow velocity along the unit magnetic vector $\mathbf{b}(z) = \mathbf{B}/|\mathbf{B}|$. The distribution function of ion flows at the boundary $f_0\left(z,\mathbf{v},n_{(\pm)},T,V_D\right)$ is sampled using the generation of $3\cdot 2^{17}$quasi-particles per second in the incoming flow. Under such conditions, the instantaneous number of particles in the system is about $1.5\cdot 10^8$. For these calculations, we consider the following parameters: ΔB_x = 40 nT, $B_z = \Delta B_x/20 = 2$ *nt*, $T = 4$ kev, $V_T \approx 619$ *km/s*, $V_D = 2V_T$, and seven values of B_y = 0, 0.5, …, 3 nT with a step 0.5 nT. The half of the system size Z_0 was taken as $Z_0 \equiv R_E$ = 6400 km ($Z_0 \gg L$; $L \approx 0.1\ R_E$), step of the space grid is $h = R_E/512$ = 12.5km. We note that for received in the simulation concentration value $n \approx 0.25$ cm^{-3} the electron skin depth $l_e = c/\omega_{pe}$ takes the value $l_e \approx 10$ km, and electron Debye length λ_{De} for the characteristic temperature T_e = 0.5 kev takes the value $\lambda_{De} \approx 0.3$ km, that is smaller than the step of the space grid h. Also we note that in the magnetic field $B \approx 20$ nT at the boundary of the CS cyclotron radius for protons and electrons take the values $R_{ci} \approx 322$ km and $R_{ce} \approx 2.7$ km, respectively.

[33] In order that self-consistent simulation should rapidly converge toward a stationary configuration, the simulation was performed in two stages. In the first stage (the so-called "self-consistent tracing" of macroparticles from the boundary of the simulation region), a nearly equilibrium TCS configuration was obtained, which served as the initial condition for the self-consistent simulation in the second stage.

[34] The self-consistent tracing was performed as follows. For the chosen set of input parameters, the initial magnetic field was specified. From the sources located close to the boundaries $|z| = 1.5Z_0$ of the system, macroparticles simulating the distribution function in plasma flows were launched. For each macroparticle its trajectory was calculated until the macroparticle left the simulation region $\{|z| < 1.5Z_0\}$. After each time interval τ_0 (in present runs τ_0 = 1/512 s) a macroparticle was "weighted"; that is, its contribution to the grid arrays was calculated using the fourth-order PQS weighting. In result ion's concentration $n(z)$, current density $\mathbf{j}(z)$ and stress tensor $\hat{\mathbf{\Pi}}(z)$ were calculated at the grid points. After this the self-consistent magnetic field component $B_x(z)$ in the next approximation were calculated. The calculations were performed until the iterative process converged, that is, until the relative change in the self-consistent magnetic field in successive iterations became sufficiently small.

[35] The second stage is the self-consistent numerical simulation using the implicit iterative scheme of the joint solution of the 1-D Ampere equation for the magnetic field and the Lorentz equations for macroparticles, and the adequate implicit algorithm for calculating the particle trajectories. In the case of a rather strong magnetic field, this algorithm is much more efficient that the "leap-frog" algorithm. This approach allowed us to use about 200 millions of model particles. Owing to the first stage, the equilibrium TCS configuration in the second stage was established rather rapidly and this equilibrium satisfied with enough good accuracy the magnetostatic equation $\mathrm{div}\hat{\mathbf{\Pi}}(z) = [\mathbf{j}(z)\times\mathbf{B}(z)]$, which yields the following force balance equations along the ***X***, ***Y***, and ***Z*** axes, respectively:

$$\Pi_{x,z}(z) - \frac{B_zB_x(z)}{\mu_0} \equiv \text{const},\ \Pi_{y,z}(z) \equiv \text{const},\ \Pi_{z,z}(z) + \frac{|B_x(z)|^2}{2\mu_0} \equiv \text{const}.$$

7. PIC Model Results

[36] Figure 9 shows the profiles of current density $j_y(z)$ (at left) and plasma concentration $n(z)$ (at right) for B_y = 3 nT as obtained from PIC simulations. The contribution from the northern source is indicated by the red line while that from the southern source is shown by the blue line. The total profile is shown by the black line. It can be seen that particles coming from the southern side can cross the TCS region without significant scattering and support the "classical" shape of current density profile with a single strong maximum in the center. In contrast, ions originating from the northern side of TCS are strongly scattered and become trapped in the TCS region. Correspondingly, the net current that they contribute is significantly reduced. More specifically, the current produced by these "Northern" Hemisphere–originating particles is characteristic of the trapped population current. It exhibits a negative excursion in the center and two positive maxima at the TCS periphery. This effect is clearly noticeable in Figure 9a where the red line corresponds to the current density of protons from the northern source. Figure 9 also reveals some deflection of the current plane from its initial position owing to small changes in TCS balance. These changes of TCS balance and deviation of TCS equilibrium position can be explained by the "north-south" asymmetry of plasma density as displayed in Figure 9b.

[37] Figure 10 shows profiles of (Figure 10a) magnetic field, (Figure 10b) current density, and (Figure 10c) plasma density for different values of guiding field. The various effects discussed above, namely, CS thickening, decrease of

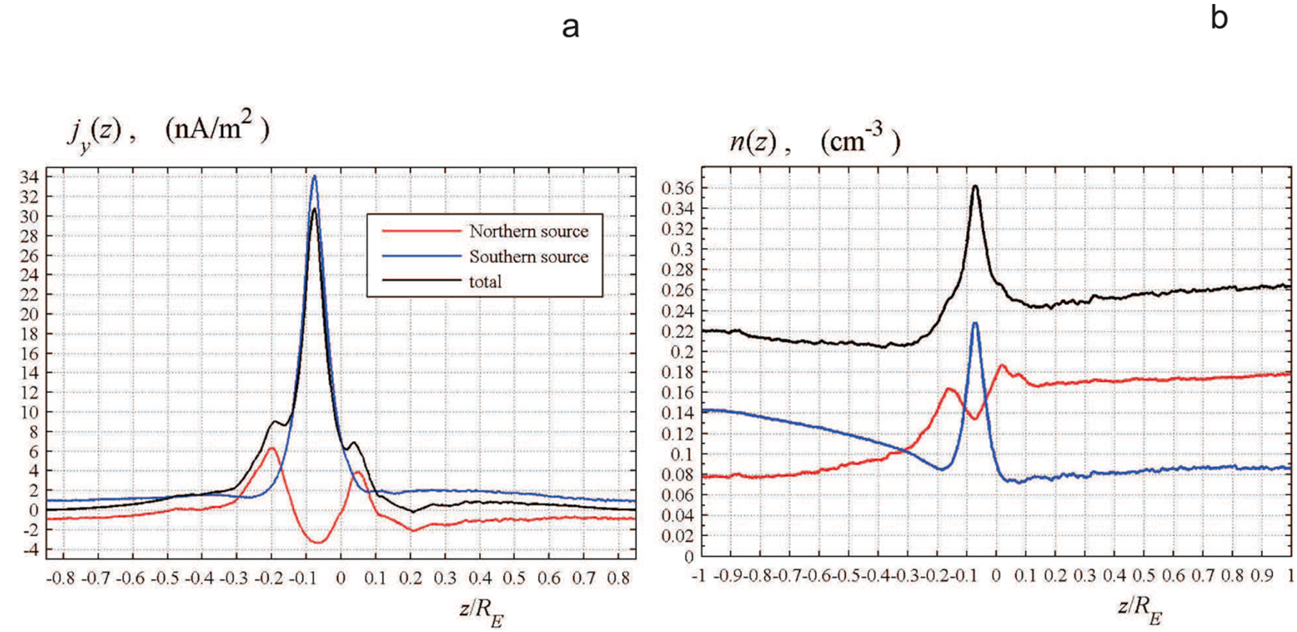

Figure 9. Profiles of (a) current density $j_y(z)$ and (b) plasma concentration $n(z)$ obtained by numerical simulation of TCS sheared equilibrium for $B_y = 3$ nT. The contribution from the northern source is shown by the red line, that from the southern source by the blue line. The total profile is shown by the black line.

the current density magnitude, and asymmetry of profiles depending upon B_y, can clearly be seen in Figure 10. On the whole, PIC numerical results are thus in a good agreement with the analytical model described in section 5. Both analytical and PIC results confirm that, in the case $j_x = j_z = 0$, thin current sheets are strongly influenced by the external magnetic shear. This shear clearly affects the particle dynamics and leads to an asymmetry of particle scattering

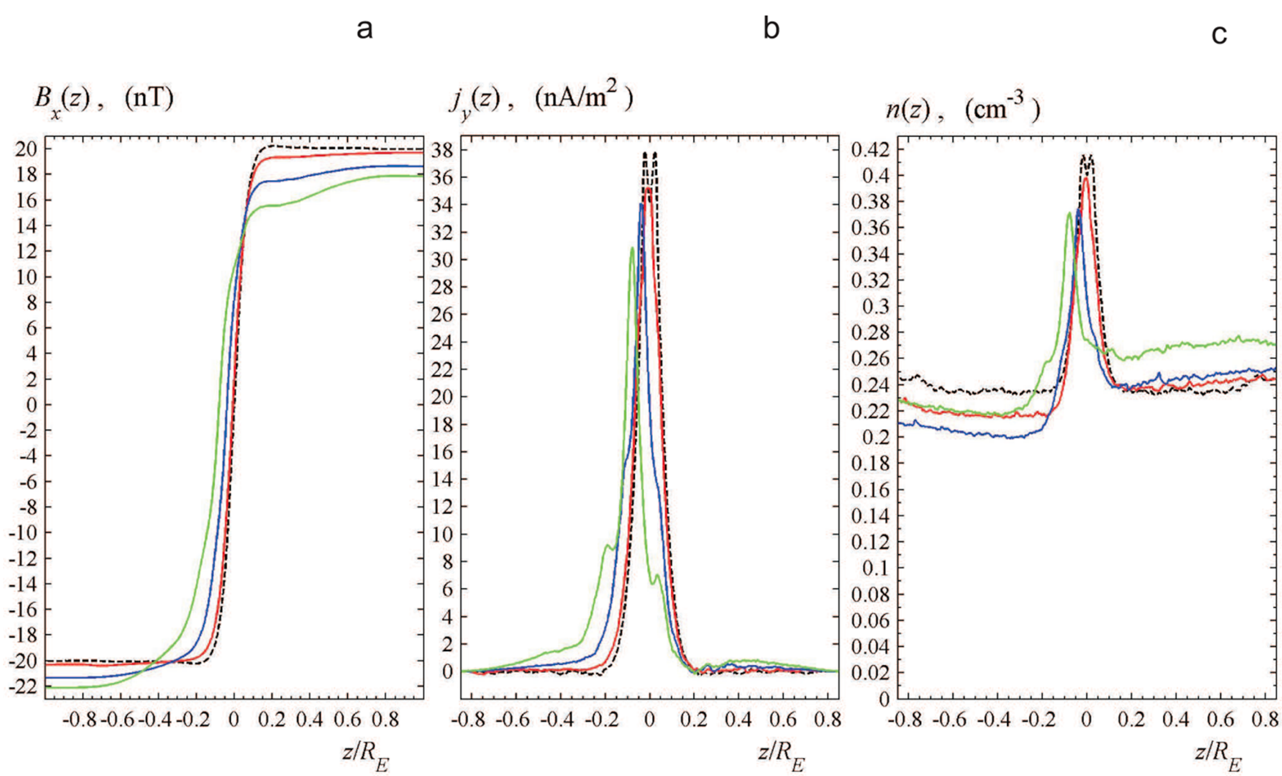

Figure 10. Profiles of (a) magnetic field component $B_x(z)$, (b) current density $j_y(z)$, and (c) plasma density $n(z)$ obtained by numerical simulation for relative values $B_y/B_z = 0$, 0.5, 1.0, 1.5 (corresponding to the dashed black, red, blue, and green lines, respectively).

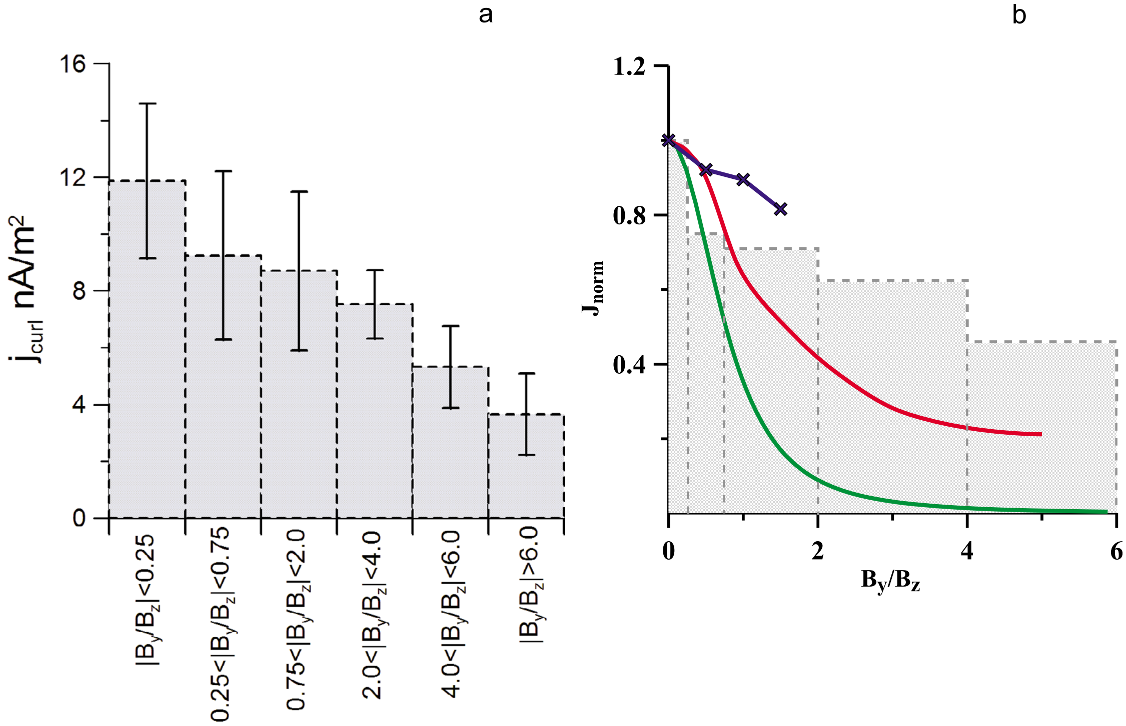

Figure 11. Maximum values of current density versus values of sheared magnetic field. (a) Current density amplitude j_{curl} obtained from Cluster via the curlometer method as a function of the B_y/B_z ratio (standard deviations are also shown). (b) Identical to Figure 11a but showing the current density $J_{norm}(B_y/B_z)$ normalized to 1 for comparison with normalized results of the semianalytical model (red line) in Figure 8b, PIC model (blue line with crosses) in Figure 10b, and analytical estimate for electron currents from section 5 (green line).

in the north-south direction. Conversely, the asymmetry of ion scattering leads to the formation of asymmetric profiles of self-consistent current density and corresponding magnetic field. The guide field also yields an effective thickening of the TCS profile.

8. Comparison of Models and Spacecraft Observations

[38] Finally, we briefly compare the above model results with Cluster observations in Earth's magnetotail. One of the main results obtained above is the decrease of the j_y amplitude with the increase of B_y (see Figure 8b). To further investigate this outcome, we use the statistics of 70 horizontal TCS crossings by Cluster in 2001, 2002 and 2004. The list of these crossings together with the main TCS parameters can be found in the work of *Artemyev et al.* [2011]. For each TCS crossing, we determine the amplitude of the current density $j_{\text{curl}} = \mathbf{e}_y(c/4\pi)\,\text{rot}\,\mathbf{B}$ and the ratio B_y/B_z in the central region where $|B_x| < 5$ nT. All current sheets from our statistics represent the relatively fast (duration less than 10 min) crossings of thin current sheets (thickness about one to three proton Larmor radius; see details in the work of *Petrukovich* [2011] and *Artemyev et al.* [2011]). During these crossings Bz component varies weakly and the averaged value of Bz can be considered as relatively reliable parameter. Details of this technique can be found in the work of *Runov et al.* [2006], *Artemyev et al.* [2008], and references therein. Then, we plot the averaged value of j_{curl} corresponding to the given value of B_y/B_z as shown in Figure 11a. In Figure 11a, one can clearly see that the growth of B_y/B_z goes together with a decrease of amplitude j_{curl} in agreement with the above model predictions. Further comparison of the theoretical results with in situ measurements (this comparison has exclusively qualitative character here) is presented in Figure 11b where all current densities are normalized to their largest values. Histogram of the normalized to maximum current density values Cluster data (filled by gray color) is shown together with the normalized results from the PIC model (blue line with crosses), from the semianalytical model (red line) and from analytical estimates for electron currents in section 5 (green line). Figure 11b is in agreement with the above analytical considerations, where one expects a fast decrease of the current density maximum owing to the decrease of the electron current (green line) in the presence of a growing values of guiding field. This effect is not accounted for in the ion PIC model, the corresponding blue line demonstrates very weak dependence from guiding field. At large values of guiding field when electron currents become negligibly small the current density continues to decrease because of enhanced ion trapping near current sheet. As we mentioned above, contrary to Speiser's ions, quasi-trapped ones do not carry significant cross-tail current. Thus the results of analytical model taking into account electrostatic effects demonstrate (red line) the domination of electron-related effect of current density decrease at smaller B_y values and slower

ion-related dependence at larger values of guiding field. One should notice that the role of electron currents in thin current sheets in the presence of guiding field is sometimes difficult to identify in Cluster observations because of insufficient space resolution of spacecraft. Still, a decrease of the current density maximum in sheared magnetic fields is clearly noticeable in both theoretical estimates and in situ measurements.

9. Conclusion

[39] We have developed two models (semianalytical and numerical) of anisotropic magnetotail current sheet, taking into account the presence of a finite guide component B_y of the magnetic field. The following conclusions can be drawn from these models:

[40] 1. TCS equilibria can exist in the presence of externally driven magnetic shear. The electron curvature current in the center of TCS decreases as $j_e \sim (1 + (B_{y0}/B_{z0})^2)^{-1}$ owing to the local increase of the field line curvature radius by magnetic shear.

[41] 2. Ion current profiles conserve the general topology and characteristic serpentine feature near the TCS center. Still, in the presence of an external B_y component, serpentine trajectories are more tangled. As a result of these changes in particle dynamics, the TCS thickness becomes substantially larger and depends upon the value of B_y.

[42] 3. Ion reflection coefficients after interaction with TCS are different for northward and southward propagation when $B_{y0} \neq 0$. Reflection coefficient for particles originating from the Northern Hemisphere does not change for the case $B_y \neq 0$, but the coefficient for Southern Hemisphere–originating particles decreases $\sim 1/B_y$ value. As a result, the profile of plasma density becomes slightly asymmetric owing to enhanced diamagnetic currents in the more populated northern region. Simultaneously, a new force balance leads to TCS deflection away from the center plane (assumed at $z = 0$ for $B_y = 0$).

[43] 4. A qualitative agreement is obtained between the modeling results and experimental data based on Cluster TCS statistics in Earth's magnetotail.

[44] **Acknowledgments.** This work is partially supported by RFBR grants 11-02-01166, 10-05-91001, 10-02-93114, NOZ 14.740.11.0086, HIII-3200.2010.2, FP-7 269198, and grant of RF Ministry of Education and Science 11.G34.31.0001 (with SPBGU and leading scientist G. S. Pavlov).

[45] Masaki Fujimoto thanks the reviewers for their assistance in evaluating this paper.

References

Alpers, W. (1971), On the equilibrium of an exact charge neutral magnetopause, *Astrophys. Space Sci.*, *11*, 471–474.
Angelopoulos, V., et al. (2008), Tail reconnection triggering substorm onset, *Science*, *321*, 931–935, doi:10.1126/science.1160495.
Arons, J. A. (2011), A tale of two current sheets, in *High-Energy Emission From Pulsars and Their Systems*, edited by N. Rea and D. F. Torres, pp. 165–180, Springer, New York, doi:10.1007/978-3-642-17251-9_13.
Artemyev, A. V., A. A. Petrukovich, L. M. Zelenyi, H. V. Malova, V. Y. Popov, R. Nakamura, A. Runov, and S. Apatenkov (2008), Comparison of multi-point measurements of current sheet structure and analytical models, *Ann. Geophys.*, *26*, 2749–2758, doi:10.5194/angeo-26-2749-2008.
Artemyev, A. V., A. A. Petrukovich, R. Nakamura, and L. M. Zelenyi (2011), Cluster statistics of thin current sheets in the Earth magnetotail: Specifics of the dawn flank, proton temperature profiles and electrostatic effects, *J. Geophys. Res.*, *116*, A09233, doi:10.1029/2011JA016801.
Asano, Y., T. Mukai, M. Hoshino, Y. Saito, H. Hayakawa, and T. Nagai (2004), Current sheet structure around the near-Earth neutral line observed by Geotail, *J. Geophys. Res.*, *109*, A02212, doi:10.1029/2003JA010114.
Ashour-Abdalla, M., L. M. Zelenyi, J. M. Bosqued, and R. A. Kovrazhkin (1992), Precipitation of fast ion beams from the plasma sheet boundary layer, *Geophys. Res. Lett.*, *19*, 617–620, doi:10.1029/92GL00048.
Ashour-Abdalla, M., L. M. Zelenyi, V. Peroomian, and R. L. Richard (1993), On the structure of the magnetotail current sheet, *Geophys. Res. Lett.*, *20*, 2019–2022, doi:10.1029/93GL01695.
Baker, D. N., T. I. Pulkkinen, V. Angelopoulos, W. Baumjohann, and R. L. McPherron (1996), Neutral line model of substorms: Past results and present view, *J. Geophys. Res.*, *101*, 12,975–13,010, doi:10.1029/95JA03753.
Baumjohann, W., et al. (2007), Dynamics of thin current sheets: Cluster observations, *Ann. Geophys.*, *25*, 1365–1389, doi:10.5194/angeo-25-1365-2007.
Birn, J., and M. Hesse (1994), Particle acceleration in the dynamic magnetotail: Orbits in self-consistent three-dimensional MHD fields, *J. Geophys. Res.*, *99*, 109–119, doi:10.1029/93JA02284.
Brittnacher, M., K. B. Quest, and H. Karimabadi (1998), A study of the effect of pitch angle and spatial diffusion on tearing instability using a new finite element based linear code, *J. Geophys. Res.*, *103*, 4587–4596, doi:10.1029/97JA03365.
Büchner, J., and L. M. Zelenyi (1986), Deterministic chaos in the dynamics of charged particles near a magnetic field reversal, *Phys. Lett. A*, *118*, 395–399, doi:10.1016/0375-9601(86)90268-9.
Büchner, J., and L. M. Zelenyi (1989), Regular and chaotic charged particle motion in magnetotaillike field reversals: 1. Basic theory of trapped motion, *J. Geophys. Res.*, *94*, 11,821–11,842, doi:10.1029/JA094iA09p11821.
Büchner, J. and L. M. Zelenyi (1991), Regular and chaotic particle motion in sheared magnetic field reversals, *Adv. Space Res.*, *11*, 177–182.
Burkhart, G. R., and J. Chen (1991), Differential memory in the Earth's magnetotail, *J. Geophys. Res.*, *96*, 14,033–14,049, doi:10.1029/91JA01137.
Chapman, S. C., and C. G. Mouikis (1996), A comparison of self-consistent kinetic and quasi-MHD simulations: Application to a dipolarizing field reversal, *Geophys. Res. Lett.*, *23*, 3251–3254, doi:10.1029/96GL02845.
Chapman, S. C., and G. Rowlands (1998), Are particles detrapped by constant B_y in static magnetic reversals?, *J. Geophys. Res.*, *103*, 4597–4603, doi:10.1029/97JA01737.
Chen, J. (1992), Nonlinear dynamics of charged particles in the magnetotail, *J. Geophys. Res.*, *97*, 15,011–15,050, doi:10.1029/92JA00955.
Chen, J., and P. J. Palmadesso (1986), Chaos and nonlinear dynamics of single-particle orbits in a magnetotail-like magnetic field, *J. Geophys. Res.*, *91*, 1499–1508, doi:10.1029/JA091iA02p01499.
Coppi, B., G. Laval, and R. Pellat (1966), Dynamics of the geomagnetic tail, *Phys. Rev. Lett.*, *16*, 1207–1210, doi:10.1103/PhysRevLett.16.1207.
Delcourt, D. C., and G. Belmont (1998), Ion dynamics at the earthward termination of the magnetotail current sheet, *J. Geophys. Res.*, *103*, 4605–4613, doi:10.1029/97JA01844.
Delcourt, D. C., L. M. Zelenyi, and J.-A. Sauvaud (2000), Magnetic moment scattering in a field reversal with nonzero B_y component, *J. Geophys. Res.*, *105*, 349–360, doi:10.1029/1999JA900451.
Frank, A. G., S. G. Bugrov, and V. S. Markov (2008), Hall currents in a current sheet: Structure and dynamics, *Phys. Plasmas*, *15*, 092102, doi:10.1063/1.2972158.
Galeev, A. A., and L. M. Zelenyi (1976), Tearing instability in plasma configurations (in Russian), *Zh. Eksp. Teor. Fiz.*, *70*, 2133–2151.
Harris, E. G. (1962), On a plasma sheath separating regions of oppositely directed magnetic fields, *Nuovo Cimento B*, *23*, 115–121, doi:10.1007/BF02733547.
Hilmer, R. V., and G.-H. Voigt (1987), The effects of magnetic B_y component on geomagnetic tail equilibria, *J. Geophys. Res.*, *92*, 8660–8672, doi:10.1029/JA092iA08p08660.
Holland, D. L., J. Chen, and A. Agranov (1996), Effects of a constant cross-tail magnetic field on the particle dynamics in the magnetotail, *J. Geophys. Res.*, *101*, 24,997–25,002, doi:10.1029/95JA02282.
Kan, J. R. (1973), On the structure of the magnetotail current sheet, *J. Geophys. Res.*, *78*, 3773–3781, doi:10.1029/JA078i019p03773.
Kaufmann, R. L., C. Lu, and D. J. Larson (1994), Cross-tail current, field-aligned current, and B_y, *J. Geophys. Res.*, *99*, 11,277–11,295, doi:10.1029/94JA00490.
Kaufmann, R. L., I. D. Kontodinas, B. M. Ball, and D. J. Larson (1997), Nonguiding center motion and substorm effects in the magnetotail, *J. Geophys. Res.*, *102*, 22,155–22,168, doi:10.1029/97JA01986.
Keiling, A., et al. (2004), New properties of energy-dispersed ions in the plasma sheet boundary layer observed by Cluster, *J. Geophys. Res.*, *109*, A05215, doi:10.1029/2003JA010277.

Keyser, J., M. Roth, J. Lemaire, B. T. Tsurutani, C. M. Ho, and C. M. Hammond (1996), Theoretical plasma distributions consistent with ULYSSES magnetic field observations in a solar wind tangential discontinuity, *Sol. Phys.*, *166*, 415–422, doi:10.1007/BF00149407.

Kropotkin, A. P., and V. I. Domrin (1996), Theory of a thin one-dimensional current sheet in collisionless space plasma, *J. Geophys. Res.*, *101*, 19,893–19,902, doi:10.1029/96JA01140.

Kropotkin, A. P., H. V. Malova, and M. I. Sitnov (1997), Self-consistent structure of a thin anisotropic current sheet, *J. Geophys. Res.*, *102*, 22,099–22,106, doi:10.1029/97JA01316.

Kuznetsova, M. M., and L. M. Zelenyi (1991), Magnetic reconnection in collisionless field reversals: The universality of the ion tearing mode, *Geophys. Res. Lett.*, *18*, 1825–1828, doi:10.1029/91GL02245.

Larson, D. J., and R. L. Kaufmann (1996), Structure of the magnetotail current sheet, *J. Geophys. Res.*, *101*, 21,447–21,461, doi:10.1029/96JA01945.

Lee, L. C., and J. R. Kan (1979), Transition layer between two magnetized plasmas, *J. Plasma Phys.*, *22*, 515–524, doi:10.1017/S002237780001028X.

Lemaire, J., and L. F. Burlaga (1976), Diamagnetic boundary layers—A kinetic theory, *Astrophys. Space Sci.*, *45*, 303–325, doi:10.1007/BF00642667.

Malova, H. V., L. M. Zelenyi, V. Popov, D. Delcourt, A. Petrukovich, and A. Runov (2007), Asymmetric thin current sheets in the Earth's magnetotail, *Geophys. Res. Lett.*, *34*, L16108, doi:10.1029/2007GL030011.

Mingalev, O. V., I. V. Mingalev, K. V. Malova, and L. M. Zelenyi (2007), Numerical simulations of plasma equilibrium in a one-dimensional current sheet with a nonzero normal magnetic field component, *Plasma Phys. Rep.*, *33*, 942–955, doi:10.1134/S1063780X07110062.

Mingalev, O. V., I. V. Mingalev, K. V. Malova, L. M. Zelenyi, and A. V. Artemyev (2009), Asymmetric configurations of a thin current sheet with a constant normal magnetic field component, *Plasma Phys. Rep.*, *35*, 76–83, doi:10.1134/S1063780X09010097.

Nakamura, R., et al. (2008), Cluster observations of an ion-scale current sheet in the magnetotail under the presence of a guide field, *J. Geophys. Res.*, *113*, A07S16, doi:10.1029/2007JA012760.

Neishtadt, A. (1987), On the change in the adiabatic invariant on crossing a separatrix in systems with two degrees of freedom, *J. Appl. Math. Mech.*, *51*, 586–592, doi:10.1016/0021-8928(87)90006-2.

Panov, E., A. Artemyev, R. Nakamura, and W. Baumjohann (2011), Two types of tangential magnetopause current sheets: Cluster observations and theory, *J. Geophys. Res.*, *116*, A12204, doi:10.1029/2011JA016860.

Pellat, R., F. V. Coroniti, and P. L. Pritchett (1991), Does ion tearing exist?, *Geophys. Res. Lett.*, *18*, 143–146, doi:10.1029/91GL00123.

Petrukovich, A. A. (2011), Origins of plasma sheet B_y, *J. Geophys. Res.*, *116*, A07217, doi:10.1029/2010JA016386.

Richardson, A., and S. C. Chapman (1994), Self-consistent one-dimensional hybrid code simulations of a relaxing field reversal, *J. Geophys. Res.*, *99*, 17,391–17,404, doi:10.1029/93JA02929.

Rong, Z. J., W. X. Wan, C. Shen, X. Li, M. W. Dunlop, A. A. Petrukovich, T. L. Zhang, and E. Lucek (2011), Statistical survey on the magnetic structure in magnetotail current sheets, *J. Geophys. Res.*, *116*, A09218, doi:10.1029/2011JA016489.

Roth, M., J. Keyser, and M. M. Kuznetsova (1996), Vlasov theory of the equilibrium structure of tangential discontinuities in space plasmas, *Space Sci. Rev.*, *76*, 251–317, doi:10.1007/BF00197842.

Runov, A., et al. (2003), Current sheet structure near magnetic X-line observed by Cluster, *Geophys. Res. Lett.*, *30*(11), 1579, doi:10.1029/2002GL016730.

Runov, A., et al. (2006), Local structure of the magnetotail current sheet: 2001 Cluster observations, *Ann. Geophys.*, *24*, 247–262, doi:10.5194/angeo-24-247-2006.

Runov, A., V. Angelopoulos, V. A. Sergeev, K.-H. Glassmeier, U. Auster, J. McFadden, D. Larson, and I. Mann (2009), Global properties of magnetotail current sheet flapping: THEMIS perspectives, *Ann. Geophys.*, *27*, 319–328, doi:10.5194/angeo-27-319-2009.

Schindler, K. (1972), A self-consistent theory of the tail of the magnetosphere, in *Earth's Magnetospheric Processes*, edited by B. M. McCormac, pp. 200–209, D. Reidel, Norwell, Mass., doi:10.1007/978-94-010-2896-7_21.

Schindler, K. (1974), A theory of the substorm mechanism, *J. Geophys. Res.*, *79*, 2803–2810, doi:10.1029/JA079i019p02803.

Sergeev, V., et al. (2003), Current sheet flapping motion and structure observed by Cluster, *Geophys. Res. Lett.*, *30*(6), 1327, doi:10.1029/2002GL016500.

Shay, M. A., J. F. Drake, and M. Swisdak (2007), Two-scale structure of the electron dissipation region during collisionless magnetic reconnection, *Phys. Rev. Lett.*, *99*, 155002.

Shen, C., Z. J. Rong, X. Li, M. Dunlop, Z. X. Liu, H. V. Malova, E. Lucek, and C. Carr (2008a), Magnetic configurations of the tilted current sheets in magnetotail, *Ann. Geophys.*, *26*, 3525–3543, doi:10.5194/angeo-26-3525-2008.

Shen, C., et al. (2008b), Flattened current sheet and its evolution in substorms, *J. Geophys. Res.*, *113*, A07S21, doi:10.1029/2007JA012812.

Sitnov, M. I., H. V. Malova, and A. T. Y. Lui (1997), Quasi-neutral sheet tearing instability induced by electron preferential acceleration from stochasticity, *J. Geophys. Res.*, *102*, 163–173, doi:10.1029/96JA01872.

Sitnov, M. I., L. M. Zelenyi, H. V. Malova, and A. S. Sharma (2000), Thin current sheet embedded within a thicker plasma sheet: Self-consistent kinetic theory, *J. Geophys. Res.*, *105*, 13,029–13,044, doi:10.1029/1999JA000431.

Sonnerup, B. U. Ö. (1971), Adiabatic particle orbits in a magnetic null sheet, *J. Geophys. Res.*, *76*, 8211–8222, doi:10.1029/JA076i034p08211.

Speiser, T. W. (1965), Particle trajectories in model current sheets: 1. Analytical solutions, *J. Geophys. Res.*, *70*, 4219–4226.

Whipple, E. C., T. G. Northrop, and T. J. Birmingham (1986), Adiabatic theory in regions of strong field gradients, *J. Geophys. Res.*, *91*, 4149–4156, doi:10.1029/JA091iA04p04149.

Yamada, M., R. Kulsrud, and H. Ji (2010), Magnetic reconnection, *Rev. Mod. Phys.*, *82*, 603–664, doi:10.1103/RevModPhys.82.603.

Zelenyi, L. M., M. I. Sitnov, H. V. Malova, and A. S. Sharma (2000), Thin and superthin ion current sheets: Quasiadiabatic and nonadiabatic models, *Nonlinear Process. Geophys.*, *7*, 127–139, doi:10.5194/npg-7-127-2000.

Zelenyi, L. M., M. S. Dolgonosov, A. A. Bykov, V. Y. Popov, and K. V. Malova (2002a), Influence of trapped plasma on the structure of collisionless thin current sheets, *Cosmic Res., Engl. Transl.*, *40*, 357–366, doi:10.1023/A:1019846428446.

Zelenyi, L. M., D. C. Delcourt, H. V. Malova, and A. S. Sharma (2002b), "Aging" of the magnetotail thin current sheets, *Geophys. Res. Lett.*, *29*(12), 1608, doi:10.1029/2001GL013789.

Zelenyi, L. M., H. V. Malova, and V. Y. Popov (2003), Bifurcation of thin current sheets in the Earth's magnetosphere, *Sov. Phys. JETP, Engl. Transl.*, *78*, 296–299, doi:10.1134/1.1625728.

Zelenyi, L. M., H. V. Malova, V. Y. Popov, D. Delcourt, and A. S. Sharma (2004), Nonlinear equilibrium structure of thin currents sheets: Influence of electron pressure anisotropy, *Nonlinear Process. Geophys.*, *11*, 579–587, doi:10.5194/npg-11-579-2004.

Zelenyi, L. M., M. S. Dolgonosov, E. E. Grigorenko, and J.-A. Sauvaud (2007), Universal properties of the nonadiabatic acceleration of ions in current sheets, *Sov. Phys. JETP, Engl. Transl.*, *85*, 187–193, doi:10.1134/S0021364007040017.

Zelenyi, L., A. Artemyev, H. Malova, and V. Popov (2008), Marginal stability of thin current sheets in the Earth's magnetotail, *J. Atmos. Sol. Terr. Phys.*, *70*, 325–333, doi:10.1016/j.jastp.2007.08.019.

Zelenyi, L. M., H. V. Malova, A. V. Artemyev, V. Y. Popov, and A. A. Petrukovich (2011), Thin current sheets in collisionless plasma: Equilibrium structure, plasma instabilities, and particle acceleration, *Plasma Phys. Rep.*, *37*, 118–160, doi:10.1134/S1063780X1102005X.

A. V. Artemyev, A. A. Petrukovich, and L. M. Zelenyi, IKI RAS, 83/32 Profsousnaya St., GSP-7, Moscow 117997, Russia.

D. C. Delcourt, Laboratoire de Physique des Plasmas, Ecole Polytechnique, CNRS, Observatoire de Saint-Maur, 4 av. de Neptune, Saint Maur des Fosses 94107, France.

H. V. Malova, Skobeltsyn Institute of Nuclear Physics, Lomonosov Moscow State University, Leninskie Gory, GSP-1, Moscow 119991, Russia. (hmalova@yandex.ru)

M. N. Mel'nik, I. V. Mingalev, and O. V. Mingalev, Institute of Applied Geophysics, Cola Scientific Center, 15 Khalturina St., Murmansk 183010, Russia. (melnik@pgia.ru; mingalev_i@pgia.ru; mingalev_o@pgia.ru)

V. Y. Popov, Physics Department, Lomonosov Moscow State University, Leninskie Gory, GSP-1, Moscow 119991, Russia. (masterlu@mail.ru)

C. Shen, Center for Space Science and Applied Research, National Space Science Center, Chinese Academy of Sciences, 1 Nanertiao, Zhongguancun, Haidian District, Beijing 8701, 100190, China.